Schweizerischer Erdbebendienst
Service Sismologique Suisse
Servizio Sismico Svizzero
Swiss Seismological Service

ETH
Eidgenössische Technische Hochschule Zürich
Swiss Federal Institute of Technology Zurich

SITE CHARACTERIZATION REPORT

SZIM: Zinal (VS), Ayer

Dario Chieppa, Vincent Perron, Donat Fäh

Last Modification: 27th January, 2021

Schweizerischer Erdbebendienst (SED)
Service Sismologique Suisse
Servizio Sismico Svizzero
Servizi da Terratrembels Svizzer
ETH Zürich
Sonneggstrasse 5
8092 Zürich
Schweiz
dario.chieppa@sed.ethz.ch

Contents

Summary

Zinal (VS) is a village located in southern Switzerland at the end of Val d'Anniviers (Canton Valais). The place was chosen as site for the installation of a new seismic station, SZIM, as part of the renewal project of the Swiss Strong Motion Network (SSMNet). In order to better assess the local subsurface, we performed a passive seismic array around the location of SZIM seismic station.

The results of the horizontal-to-vertical spectral ratio (H/V) show curves with three peaks: (1) at about 0.45 Hz, (2) between 3.0 and 3.9 Hz and (3) between 8.7 and 15.0 Hz. The second and third peaks are interpreted as the fundamental and first higher mode peaks, respectively. No picking is performed for the peak at low frequency. All peaks are divided by troughs, located at about 2.0 and 5.0 Hz.

The inversion of the passive seismic array measurements is performed using two different codes: *dinver* and Neopsy. The first one, using parametrizations with an increasing number of layers, allowed the estimation of velocity profiles down to 200 m; the second one parametrizes a 1-D layered velocity model able to investigate the subsurface down to 193 m.

Two interfaces are distinguished for all velocity profiles at about 6.5 and 48 meters. The bedrock, identified by *dinver* profiles and by the Maximum Likelihood model (ML) from Neopsy, is located between 167.6 and 193.4 meters and has S-wave velocity between 1790 and 2254 m/s. The model with the Maximum A Posteriori (MAP) probability doesn't show any half-space interface but a thick layer with S-wave velocity of 1587 m/s.

The V_{S30} value of the site is 460.2 m/s, corresponding to soil class B in EC8 and C in SIA261. The theoretical shear-wave transfer functions from the estimated V_S profiles predict an amplification function in quite good agreement in terms of amplitude with the empirical function recorded at SZIM station between 2.3 and 22.3 Hz.

1 Introduction

The station SZIM is part of the Swiss Strong Motion Network (SSMNet). The station was installed on 4 June 2019 in the framework of the second phase of the Swiss Strong Motion Network (SSMNet) renewal project (Fig. 1). In order to better characterize the underground, to estimate the fundamental frequency of the site and the shear wave velocity a passive array measurement was carried out on 22 July 2021.

The station is installed at the end of Anniviers valley (VS) in a tourist area. The installation improves the network coverage of southern Switzerland filling the gap between the stations DIX, SZEK and SNIB.

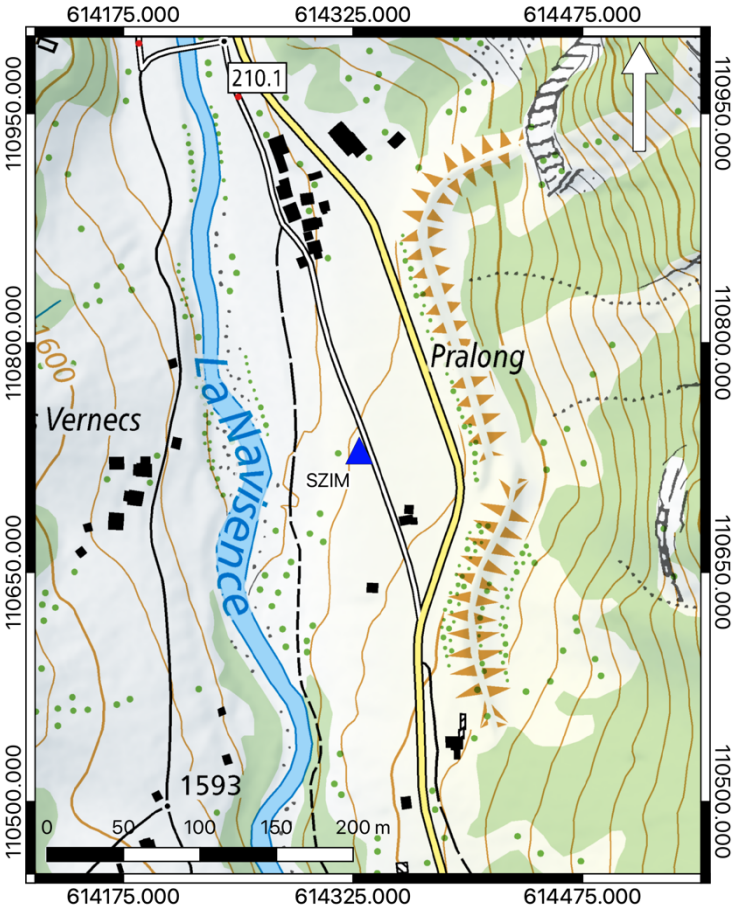

Figure 1: Map showing the location of the strong motion station (blue triangle) in Zinal. Source: Federal Office of Topography.

2 Geological setting

A geological map of the surroundings of Zinal is shown in Fig. 2. Red dots represent the location of the passive array measurement, the blue triangle the location of SZIM station. The sensors were installed on two geological units: undifferentiated alluvial deposits (Holocene) and moraine deposits (Late Pleistocene). Towards east, the unit in light blue (Fig. 2) consists in undifferentiated artificial deposits (Holocene). The seismic station SZIM is located on moraine sediments as the center of the array and the two inner rings. Only the most eastern station (SZIM48) is located on artificial sediments. Underneath the shallowest sediments, the tectonic units of Silviez-Mischabel and the Combin zone (Tsate cover) exist and are located towards north and south, respectively.

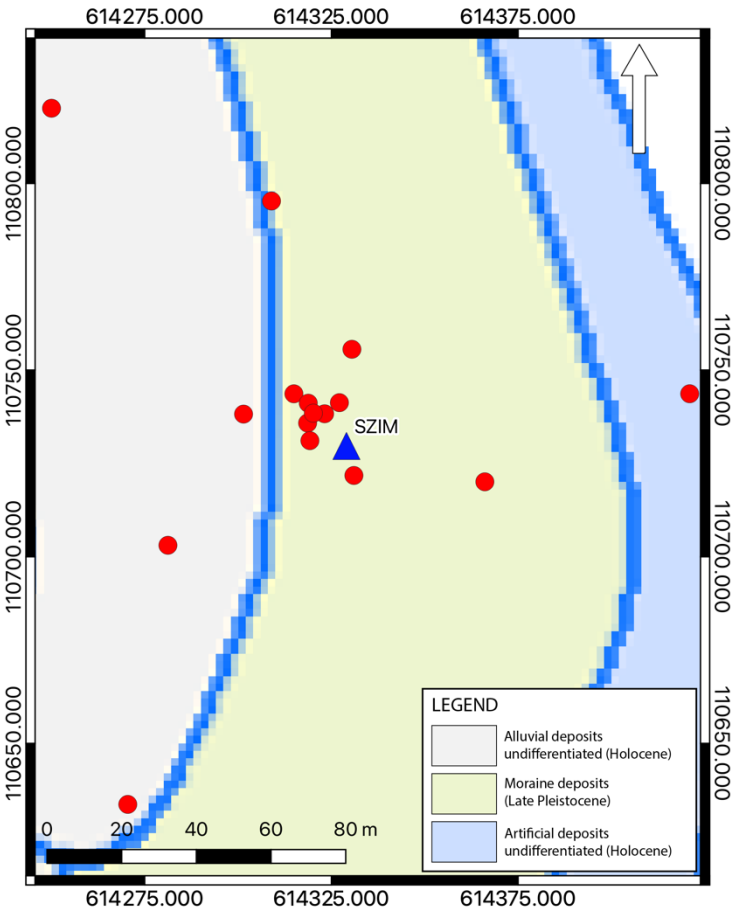

Figure 2: Geological map of the Zinal area. The stations of the passive array recordings are indicated by red dots, whereas the position of the strong-motion station SZIM is shown by a blue triangle. Source: Federal Office of Topography.

3 Passive site characterization measurements

3.1 Data set

To characterize the deep underground structure around the seismic station, a passive seismic measurement and a H/V single point measurement at the location of SZIM station were performed in July 2021.

A seismic array of 16 stations was installed (Fig. 4). The stations were planned to be located on five rings of different radii around a central station. The three stations of each ring were planned to be rotated 120 degrees one from the other. The stations of the outer ring were rotated between 115 and 125 due to the morphology. The radii of the rings are 3, 7.5, 20, 50 and 160 meters. The array central station (SZIM66) is located at about 11 m north-west from the SZIM station. Each ring, starting from the second, was rotated with respect to the inner ring of 25, 35, 20 and 30 degrees.

Each station consisted of a Lennartz 5s sensor connected to a Centaur digitizer, with the exception of four stations in the central part which had two sensors connected to the same digitizer. The station names of the array are composed of "SZIM" followed by a two-digit number between 42 and 49, 52 and 55, 63, 65, 66 and 75 (corresponding to the Centaur digitizer serial number for numbers lower than 60 plus 20 to distinguish the use of the second channel). The array recording time was 209 minutes (12540 s). The station locations were measured by a differential GPS system (Leica Viva GS10) which was set up to measure with a precision better than few centimeters.

Close to the location of SZIM station (around 50 cm), a single H/V point (SZIM1) was measured for 45 minutes.

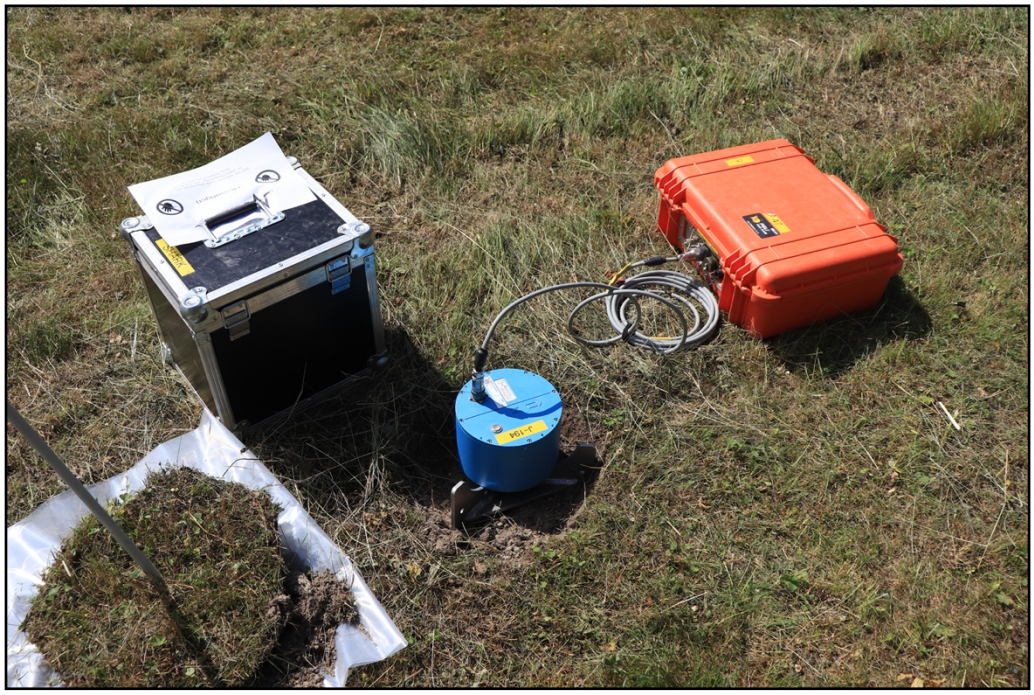

Figure 3: Seismic station installation example for the measurements in Zinal.

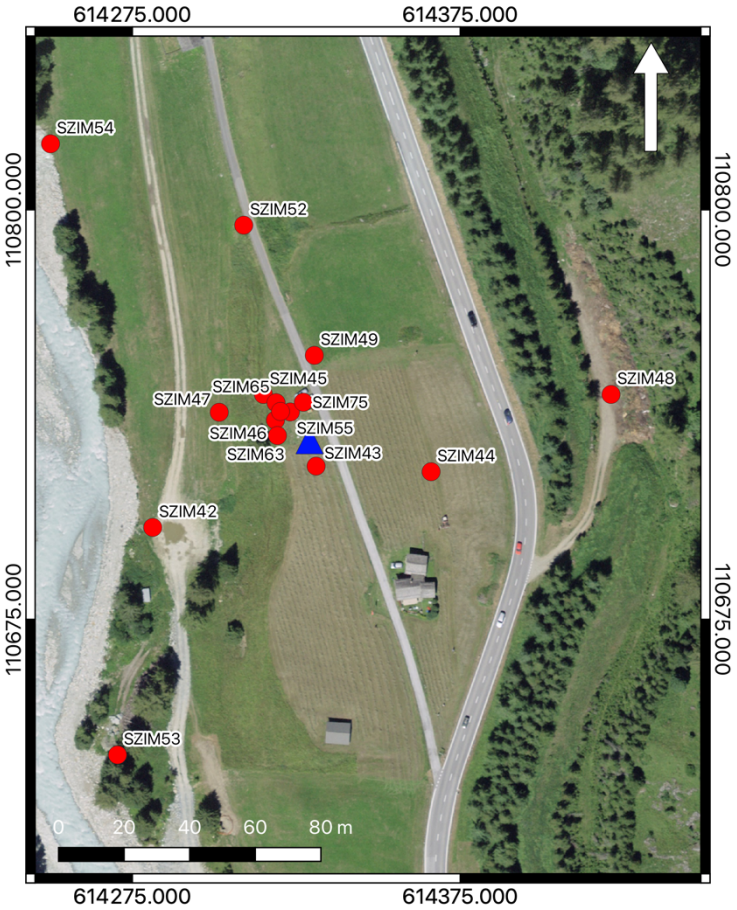

Figure 4: Layout of the array measurement in Zinal. The locations of the stations for the passive seismic measurement are indicated by the red dots. The blue triangle indicates the seismic station site. Source: Federal Office of Topography.

3.2 H/V and RayDec ellipticity curves

Figure 5, left plot, shows the H/V curves determined with the time-frequency analysis method (Fäh et al., 2009) for all stations of the passive array. The computed H/V curves do not perfectly match the ones with the others due to the uneven morphology. Common features can be recognized for most of the H/V curves: a small peak and a gently dipping trend, a trough at about 2 Hz, a broad peak and a second trough at about 5 Hz followed by a second broader peak. The first peak is located in a narrow frequency range between 3.03 and 3.89 Hz and it is interpreted as the H/V fundamental peak (red crosses); the second peak is located between 8.65 and 14.96 Hz (blue crosses) and it can be seen only by the stations in the center and in the western part of the array. The distribution of the H/V peaks is shown in Fig. 6 for the fundamental and the first higher modes, left and right respectively. At about 0.45 Hz, a third small peak can be seen. It, recognized by most of the H/V curves, was not picked since not clearly distinguishable in the Fourier spectra.
For what concerns the trough on the left (around 2 Hz), it looks narrow and deep in the center of the array (e.g. SZIM66, SZIM75, SZIM63, etc.) and wider in the outer rings. The second trough between 4.8 and 5.1 Hz has similar shape over the entire study area but different H/V values.

The RayDec technique (Hobiger et al., 2009) is meant to eliminate the contributions of other wave types than Rayleigh waves and give a better estimate of the ellipticity. The RayDec ellipticity curves for all stations of the array measurements are shown in Figure 5 (right plot). These curves show a pattern similar to the H/V curves with the exception of few curves looking almost flat at low frequency. The dark green curve indicates the array central station (SZIM66), while the dark red curve shows the RayDec ellipticity measured close to SZIM station.

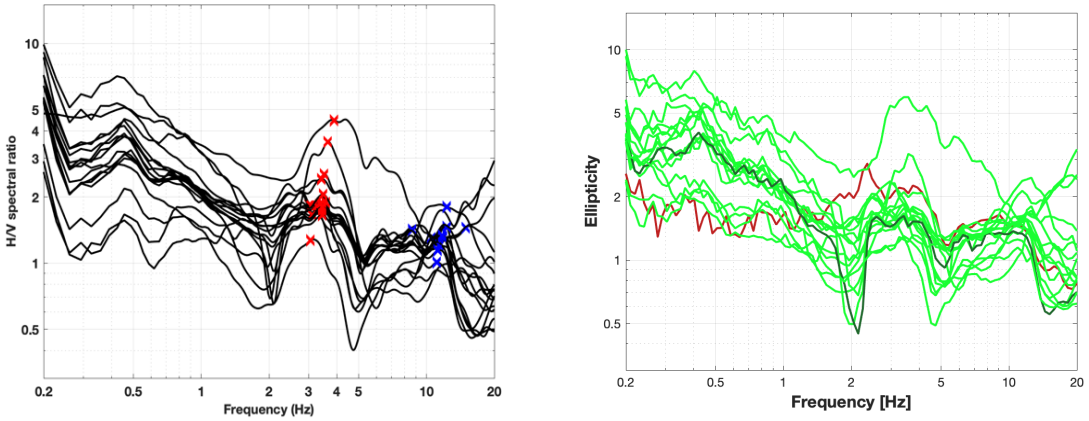

Figure 5: Left: H/V curves of the different stations of the array measurements in Zinal with picked fundamental frequency (red cross). Right: RayDec ellipticities for all stations of the array. The curve of SZIM66, the array center, is highlighted in dark green, whereas the curve SZIM1, linked to the measurement nearby the station is highlighted in dark red.

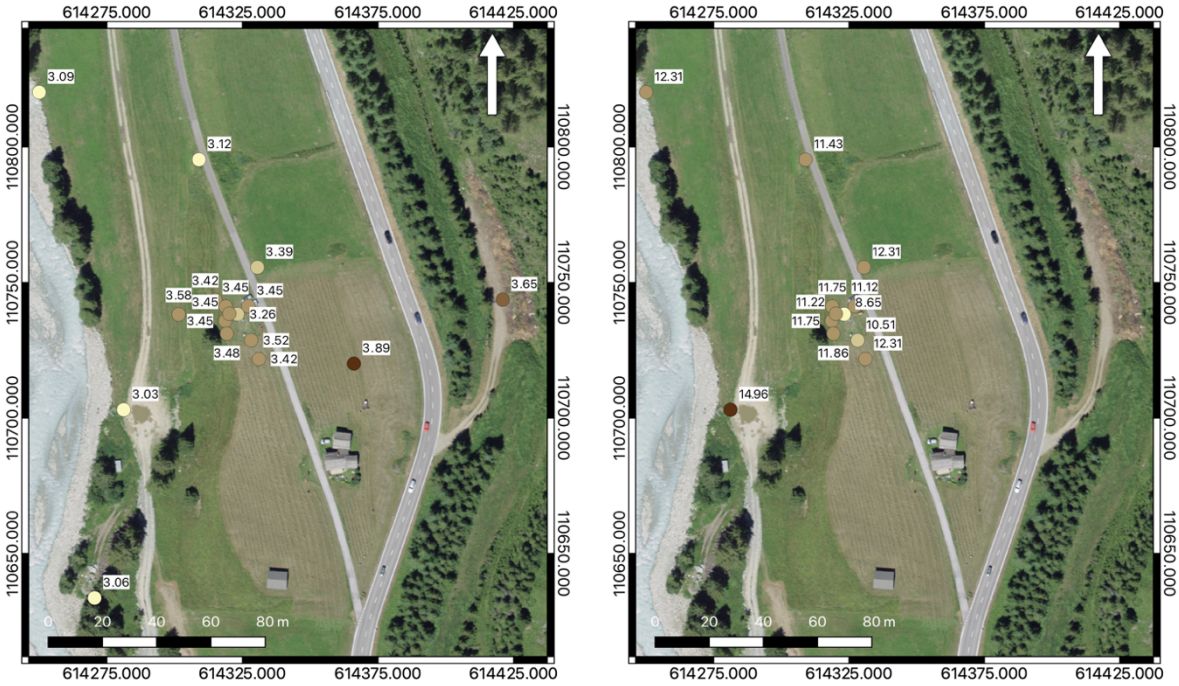

Figure 6: Map showing the variation in frequency for the H/V fundamental peak (left) and for the first higher peak (right) over the area of Zinal. Source: Federal Office of Topography.

3.3 Polarization measurements

The polarization analysis was performed according to Burjánek et al. (2010) and Burjánek et al. (2012). The results for all stations of the array are similar with the exception of station SZIM44 (not shown), which shows values of ellipticity of about 0 over the entire frequency range and two strong directions of polarization: N-S and E-W. The results are probably linked to the wrong deployment of the sensor on the tripod. At the remaining stations, the ground motion is linear and horizontally polarized at 3-4 Hz, around the H/V peak (Fig. 7 – left plot). One direction of polarization, coherent with the axis of the valley, can be seen at all sites at about 3-4 Hz. To some sites, a second direction of polarization, weaker than the first one and with an angle between 70 and 90 degrees, can be seen at low frequency (Fig. 7 – right plot). This direction, perpendicular to the axis of the valley, is probably linked to a secondary resonance effect of the valley.
The results for SZIM66, the array center, and SZIM1, the H/V point measured close to SZIM permanent station, are shown in Fig. 7 in the top and bottom lines, respectively.

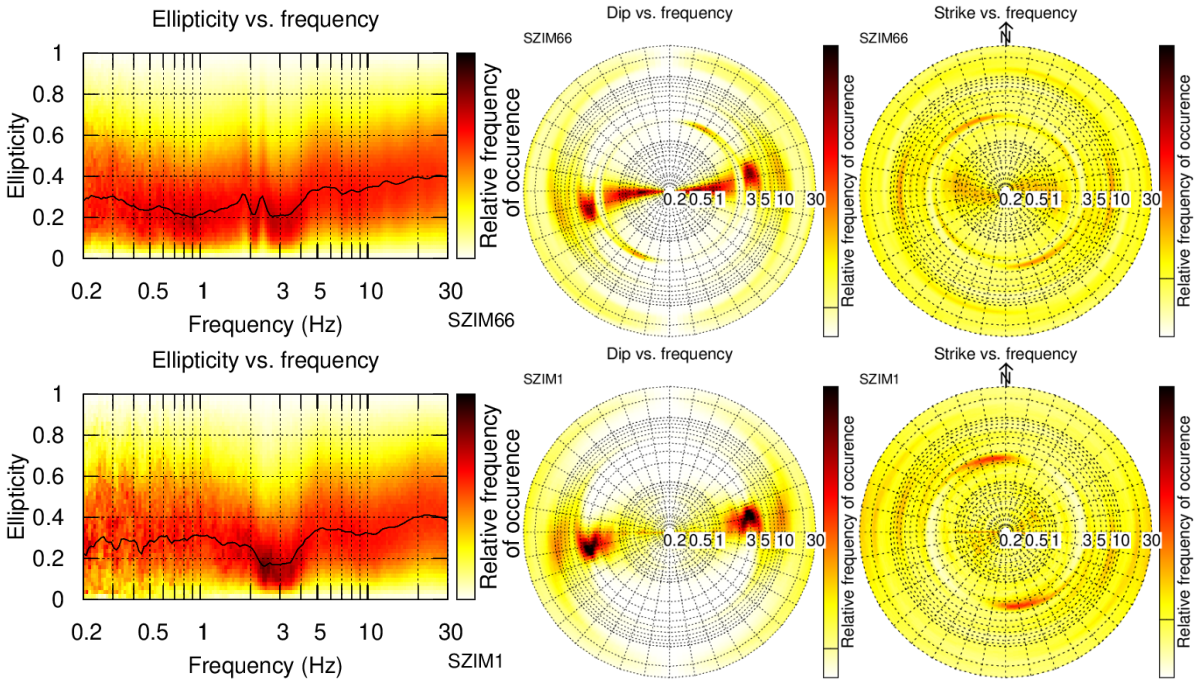

Figure 7: Polarization analysis of station SZIM66 (top line) and SZIM1 (bottom line).

3.4 3-component high-resolution FK

The results of the 3-component high-resolution FK analysis (Poggi and Fäh, 2010) are shown in Fig. 8. For Love waves, using the transverse component, a dispersion curve was picked between 2.81 and 42.2 Hz. For Rayleigh waves, we used the dispersion curves computed using the vertical and the radial components. A dispersion curve was picked using the vertical component between 4.26 and 47.26 Hz. Over the same frequency range, an ellipticity curve was picked; it shows a gradual increase in ellipticity with a wide peak between 10 and 20 Hz followed by a trough. For the radial component, one unclear but continuous dispersion curve was picked between 3.27 and 26.88 Hz. The corresponding ellipticity curve shows a wide trough and a wide peak.

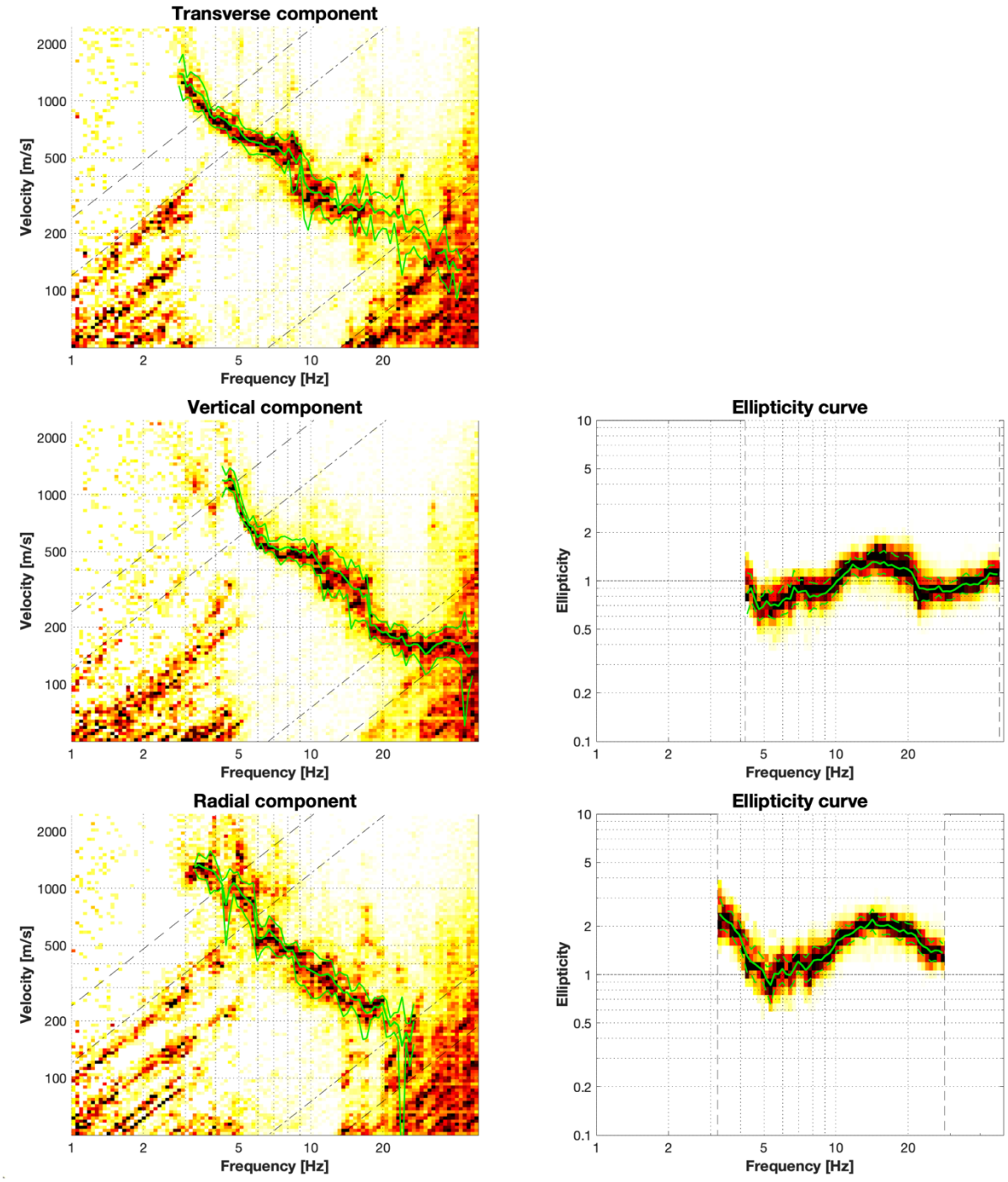

Figure 8: Dispersion curves (left column) and ellipticity curves (right column) for the transverse (top row), vertical (middle row) and radial (bottom row) components obtained with the 3-component HRFK algorithm (Poggi and Fäh, 2010). The dashed and dotted black lines are the array resolution limits. The solid and dashed green lines represent the data picking (central line) and the standard deviation (outer lines).

3.5 WaveDec

The results of the WaveDec (Maranò et al., 2012) processing are shown in Fig. 9. This technique estimates the properties of single or multiple waves simultaneously with a maximum likelihood approach. In order to get good results, the parameter γ must be tuned to modify the sharpness of the wave property estimation between purely maximum likelihood estimation and a Bayesian Information Criterion. Here, a value of $\gamma = 0.5$ was used, corresponding to a mix of Bayesian Information Criterion estimation and Maximum Likelihood.

The picking of dispersion curves in WaveDec was performed in the wavenumber-frequency domain. Fig. 9, top row, shows the dispersion curves picked for the Love waves between 3.6 and 27.2 Hz and for the Rayleigh waves between 4.6 and 22.3 Hz. While the dispersion curve for the Rayleigh wave shows a continuous curve with limited scatter, the Love wave dispersion curve, due to the shortage of points at low frequency, shows an abrupt change in slope. Over the same frequency range as the Rayleigh wave dispersion curve, the ellipticity angle was picked (Fig. 9 – bottom row). It shows positive ellipticity values below 5.1 Hz close to the lower array limit and negative above. The particle motion changes from prograde at about 5 Hz to retrograde.

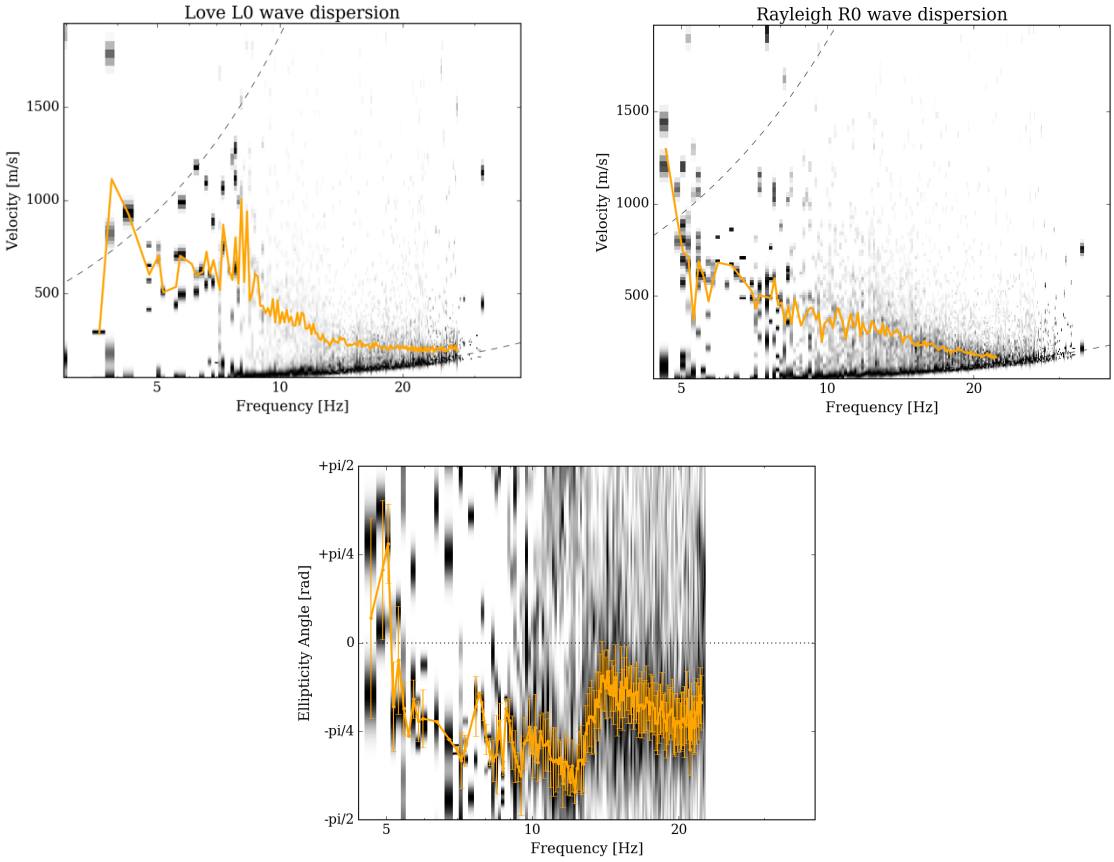

Figure 9: Dispersion curves for Love and Rayleigh waves (top row) and ellipticity angle curve for Rayleigh waves (bottom row) as obtained with WaveDec (Maranò et al., 2012). The dashed black lines in the dispersion curves plots (top rows) represent the array resolution limits, the solid orange line indicates the picked curve and the vertical bars at each frequency show the standard deviation for the ellipticity angle curve.

3.6 Modified SPatial AutoCorrelation

The SPAC (Aki, 1957) curves of the vertical components have been calculated using the MSPAC (Bettig et al., 2001) technique implemented in geopsy (Wathelet et al., 2020). Rings with different radius ranges are defined and for all stations pairs with distances inside this radius range, the cross-correlation is calculated in different frequency ranges. These cross-correlation curves are averaged for all station pairs of the respective ring and give the SPAC curves. The rings are defined in such a way that at least three station pairs contribute and that their connecting vectors have a good directional coverage.

The SPAC Autocorrelation curves are shown in Fig. 10 for all 19 rings (central and right columns). The black points indicate the data values which contributed to the final dispersion curve estimation, which was picked using *spac2disp* of the geopsy. One dispersion curve was picked for the Rayleigh wave between 3.6 and 18.3 Hz as shown by the dark gray curve in Fig. 10 (left).

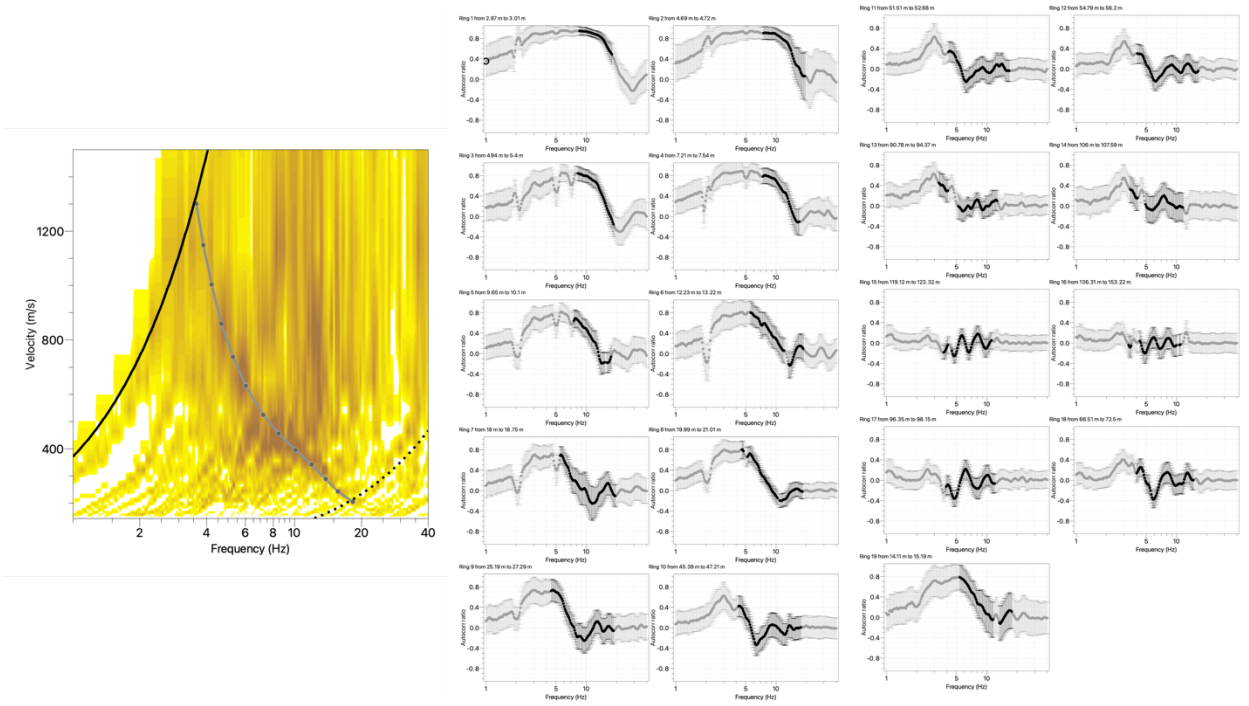

Figure 10: Rayleigh wave dispersion curve (left) obtained using spac2disp module of geopsy and autocorrelation functions for all rings (center and right). The solid gray line represents the picked data; the black dashed and dotted lines indicate the array resolution limits.

3.7 Summary

Figure 11 gives an overview of the Love and Rayleigh wave dispersion (left and central plots, respectively) and of the Rayleigh wave ellipticity curves (right plot) determined using different approaches. For Love waves, WaveDec and 3C-HRFK techniques produce one dispersion curve each with good overlap in the frequency range 4-13.5 Hz; at higher frequency, the two curves create an eye-shape structure reconnecting at about 27 Hz. For the Rayleigh waves, four curves were picked using 3C-HRFK, WaveDec and MSPAC techniques. The first method provided similar dispersion curves for the vertical (4.2 – 47.3 Hz) and radial (3.3-26.9 Hz) components. The

dispersion curves picked using WaveDec and MSPAC perfectly overlap with the other two curves. Given the presence of one dispersion curve for the Love wave and one for the Rayleigh waves, both curves are interpreted as fundamental modes.
The ellipticity curves retrieved using different methods show similar features in the frequency range 3 – 25 Hz (Fig. 11 – right plot). The RayDec curves shown for the central station (SZIM66) and for the permanent station (SZIM1) have a similar pattern above 3 Hz where a sequence of trough-peak-trough can be distinguished. At lower frequencies, the dark green curve shows a wide peak, already visible in most of the H/V curves, and a deep trough, while the light green curve shows an almost flat curve with ellipticity of 2. The RayDec curves are in agreement with the ellipticity curve computed using the radial component between 3 and 10 Hz. The ellipticity curve for the vertical component instead shows similar shape but much lower values.
The WaveDec ellipticity angle is picked between 4.6 - 22 Hz and overlaps with the RayDec curves.

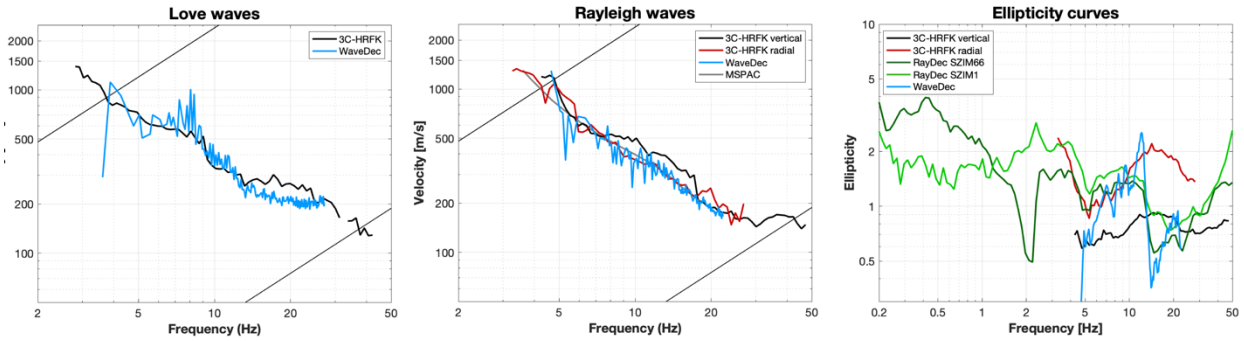

Figure 11: Comparison between the computed Love (left) and Rayleigh (center) wave dispersion curves and ellipticity curves (right).

4 Data inversion

4.1 Inversion targets

We performed several inversions using all available information. The details of the inversion targets are indicated in Table 1 and the corresponding curves are shown in black in Fig. 12.
In the inversion process, we inverted two dispersion curves and one Rayleigh wave ellipticity curve. The dispersion curves, one for the Rayleigh waves and one for the Love waves, were both interpreted as fundamental modes and selected using the results of 3C-HRFK. The ellipticity curve is the result of RayDec curve measured for the central station (SZIM66).

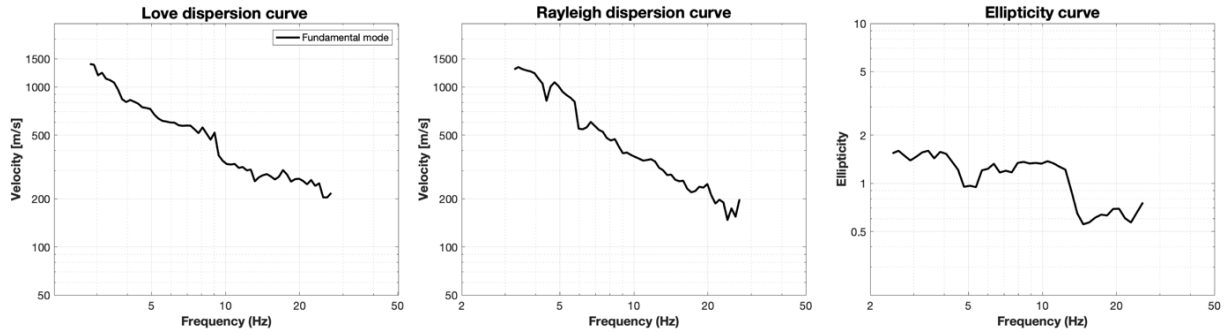

Figure 12: Overview of the dispersion curves used as target for the different inversions.

Table 1: List of the curves used as target in the inversion.

Method	Wave type	Mode	Curve type	Frequency range [Hz]
3C-HRFK	Love	fundamental	dispersion	2.81-26.88
3C-HRFK	Rayleigh	fundamental	dispersion	3.27-26.88
RayDec (SZIM66)	Rayleigh	fundamental	ellipticity	2.46-25.60

4.2 Inversion parameterization

For the inversion, five different parameterizations were tested. The first four involve free values of thickness and velocities for the different layers, ranging from 3 to 9 layers over the half-space. The S- and P-wave velocities are allowed to range from 50 to 3000 m/s and from 100 to 7000 m/s, respectively. The deepest layer interfaces were allowed to range to a depth of 200 m for all parameterizations. The density was fixed to 2300 kg/m^3 for the bedrock layer and to 2000 kg/m^3 for all the other layers.

The last parametrization had fixed layer thicknesses and consists of 18 layers over the half-space, with the deepest interface at 200 m depth. Equal ranges were defined for the P- and S-wave velocities. The density was set to increase from the surface to the half-space starting at 2000 kg/m^3 for the first layer and progressively increasing up to 2500 kg/m^3.

4.3 Inversion results - *dinver*

We performed 5 inversions with different parameterizations (see Table 2) using the Dinver routine (http://www.geopsy.org/). The targets, as reported in Table 1, are the Rayleigh and Love wave dispersion curves and the Rayleigh wave ellipticity curve in terms of ellipticity angle. Each inversion run produced 280000 models in totals in order to assure a good convergence of the solution. The results of these inversions are shown in Figs. 13 – 17.

Table 2: List of inversions

Inversion	Number of layers	Number of models	Minimum misfit
SZIM 3l	3	280000	0.563
SZIM 5l	5	280000	0.554
SZIM 7l	7	280000	0.556
SZIM 9l	9	280000	0.565
SZIM fix	18	280000	0.657

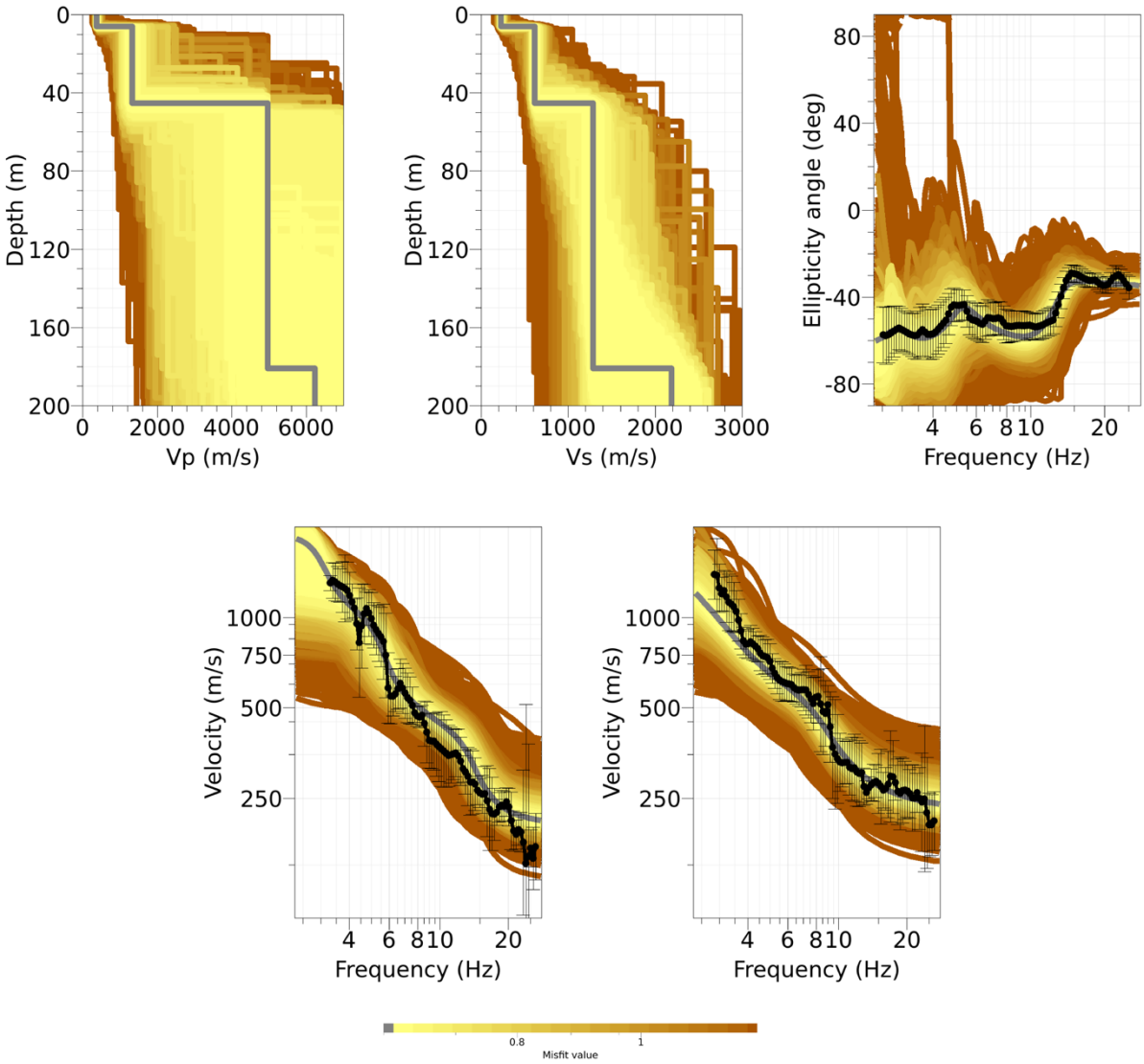

Figure 13: Inversion SZIM 3l. Top line: P-wave velocity profiles (left), S-wave velocity profiles (center) and Ellipticity angle (right). Bottom line: Dispersion curves for the fundamental mode of Rayleigh (left) and Love (right) waves. The black dots indicate the data points used for the inversion, the black bars the standard deviation of the inverted curve, while the gray line shows the best-fitting model.

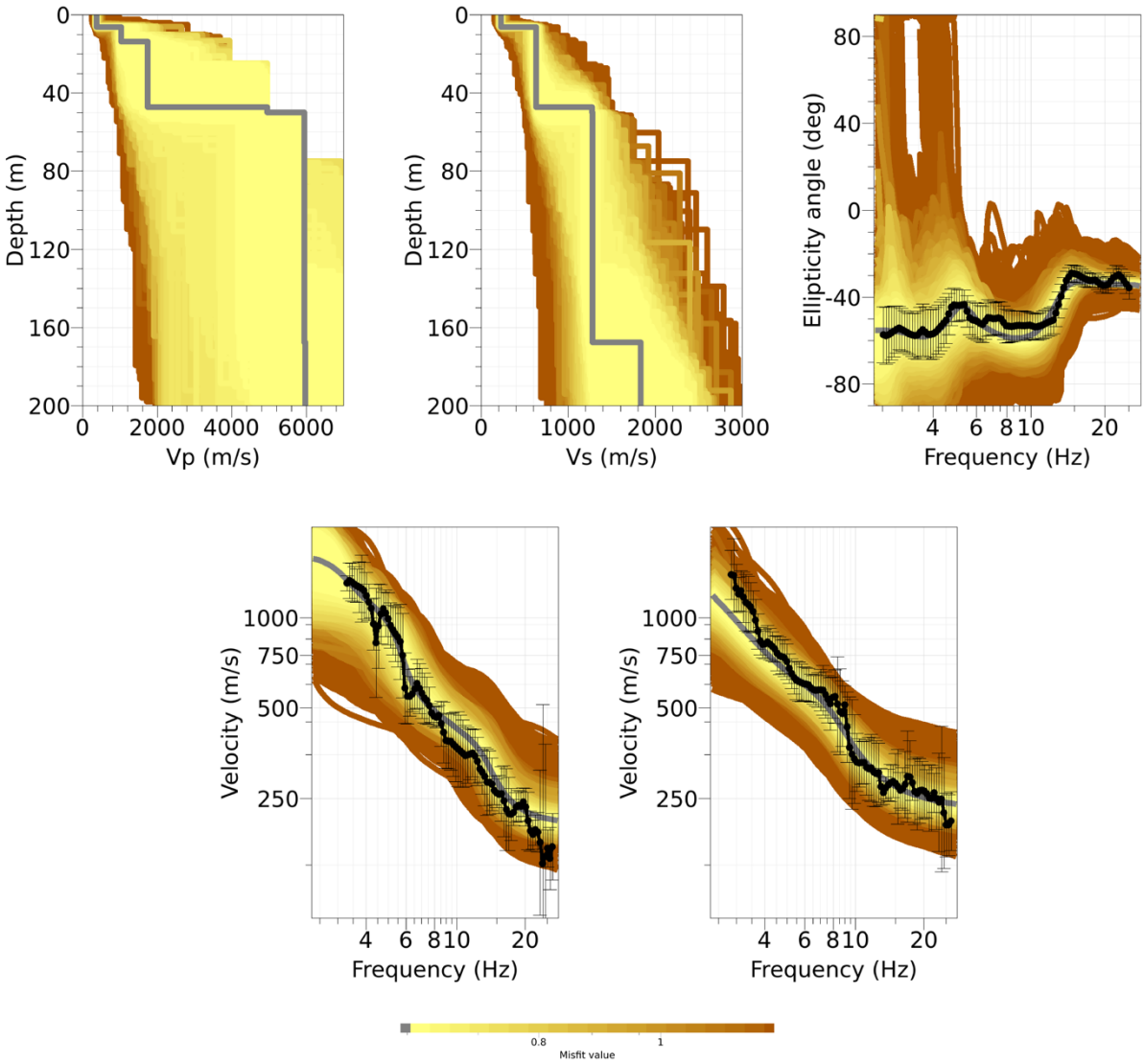

Figure 14: Inversion SZIM 5l. Top line: P-wave velocity profiles (left), S-wave velocity profiles (center) and Ellipticity angle (right). Bottom line: Dispersion curves for the fundamental mode of Rayleigh (left) and Love (right) waves. The black dots indicate the data points used for the inversion, the black bars the standard deviation of the inverted curve, while the gray line shows the best-fitting model.

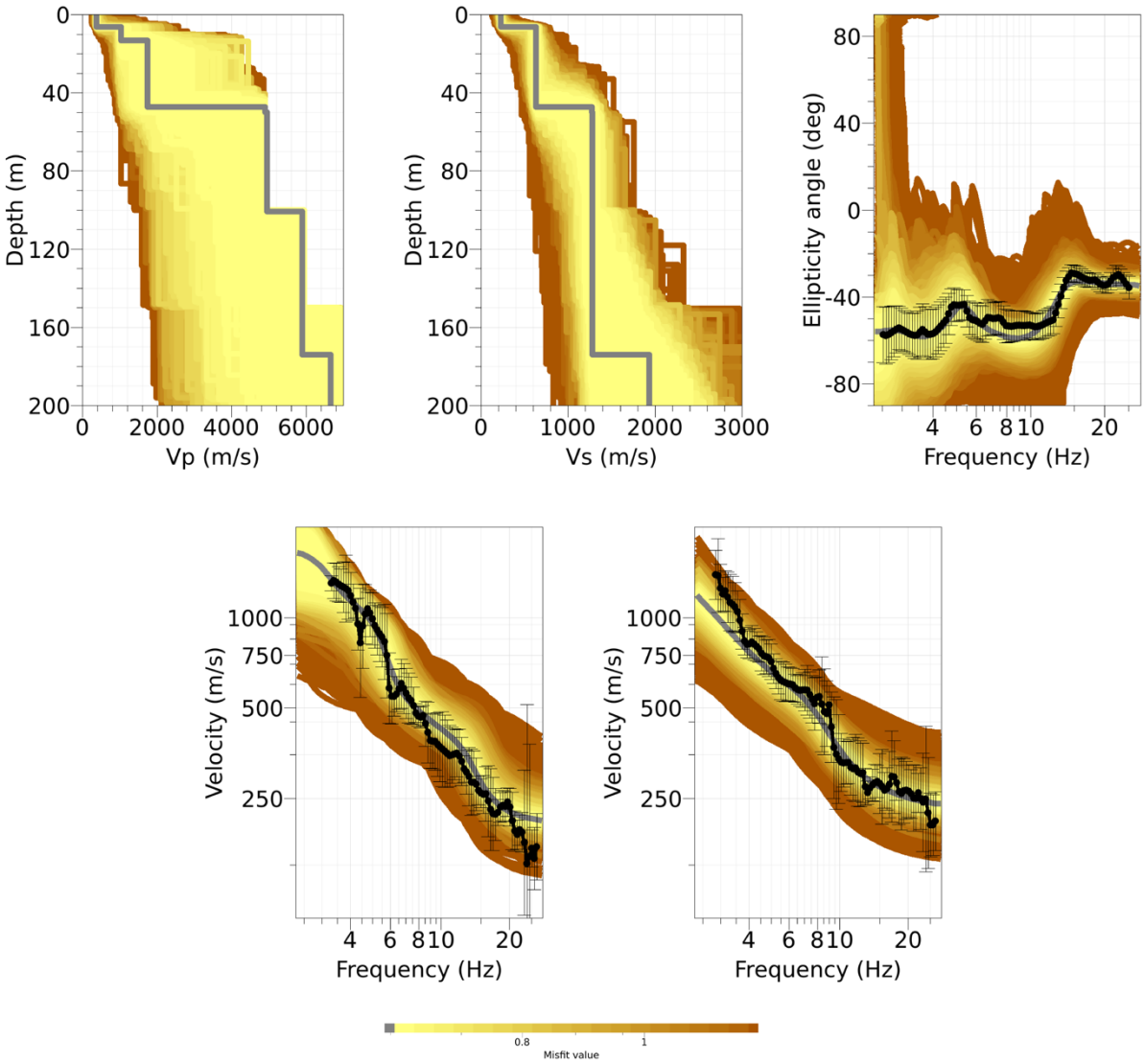

Figure 15: Inversion SZIM 7l. Top line: P-wave velocity profiles (left), S-wave velocity profiles (center) and Ellipticity angle (right). Bottom line: Dispersion curves for the fundamental mode of Rayleigh (left) and Love (right) waves. The black dots indicate the data points used for the inversion, the black bars the standard deviation of the inverted curve, while the gray line shows the best-fitting model.

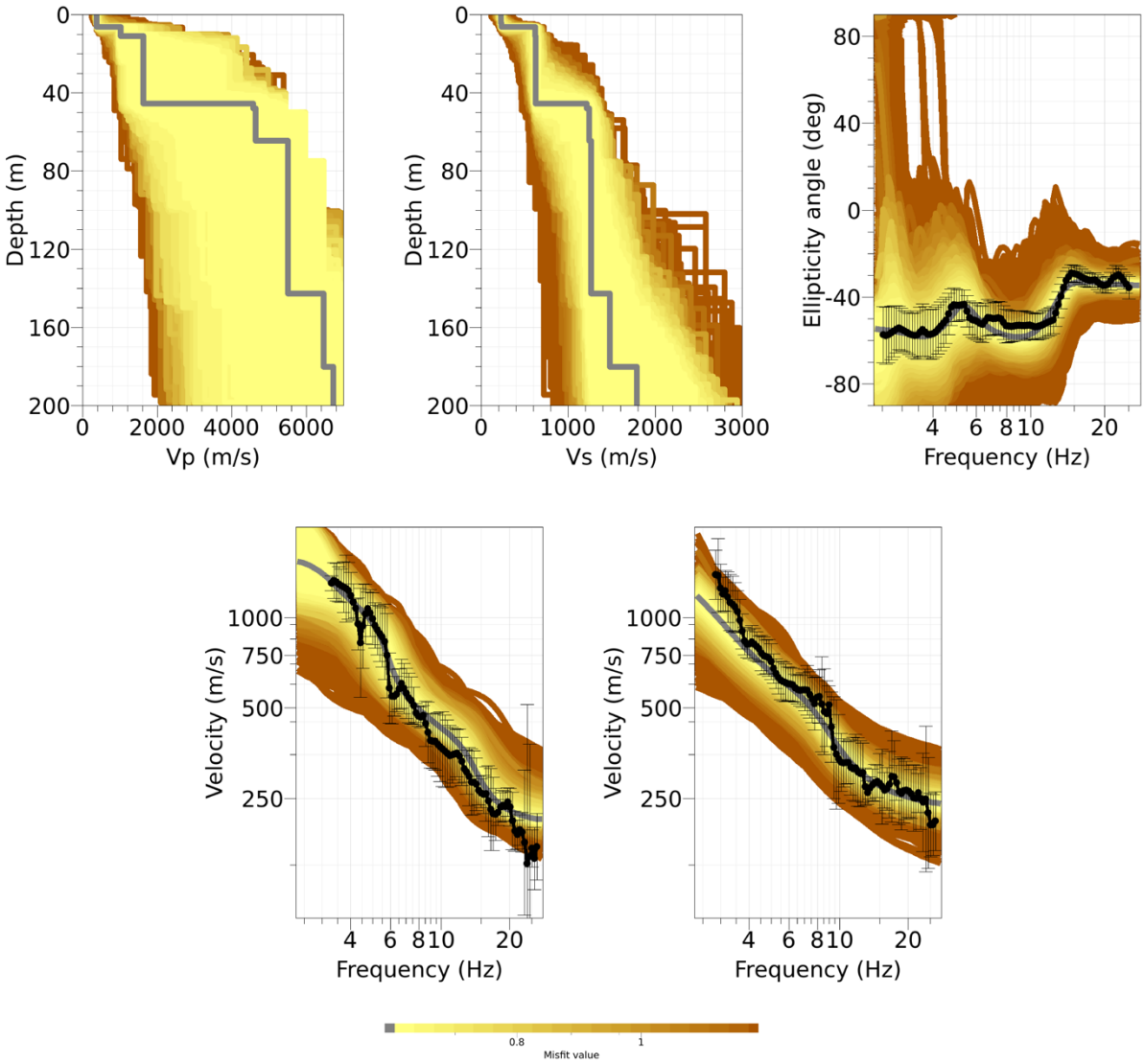

Figure 16: Inversion SZIM 9l. Top line: P-wave velocity profiles (left), S-wave velocity profiles (center) and Ellipticity angle (right). Bottom line: Dispersion curves for the fundamental mode of Rayleigh (left) and Love (right) waves. The black dots indicate the data points used for the inversion, the black bars the standard deviation of the inverted curve, while the gray line shows the best-fitting model.

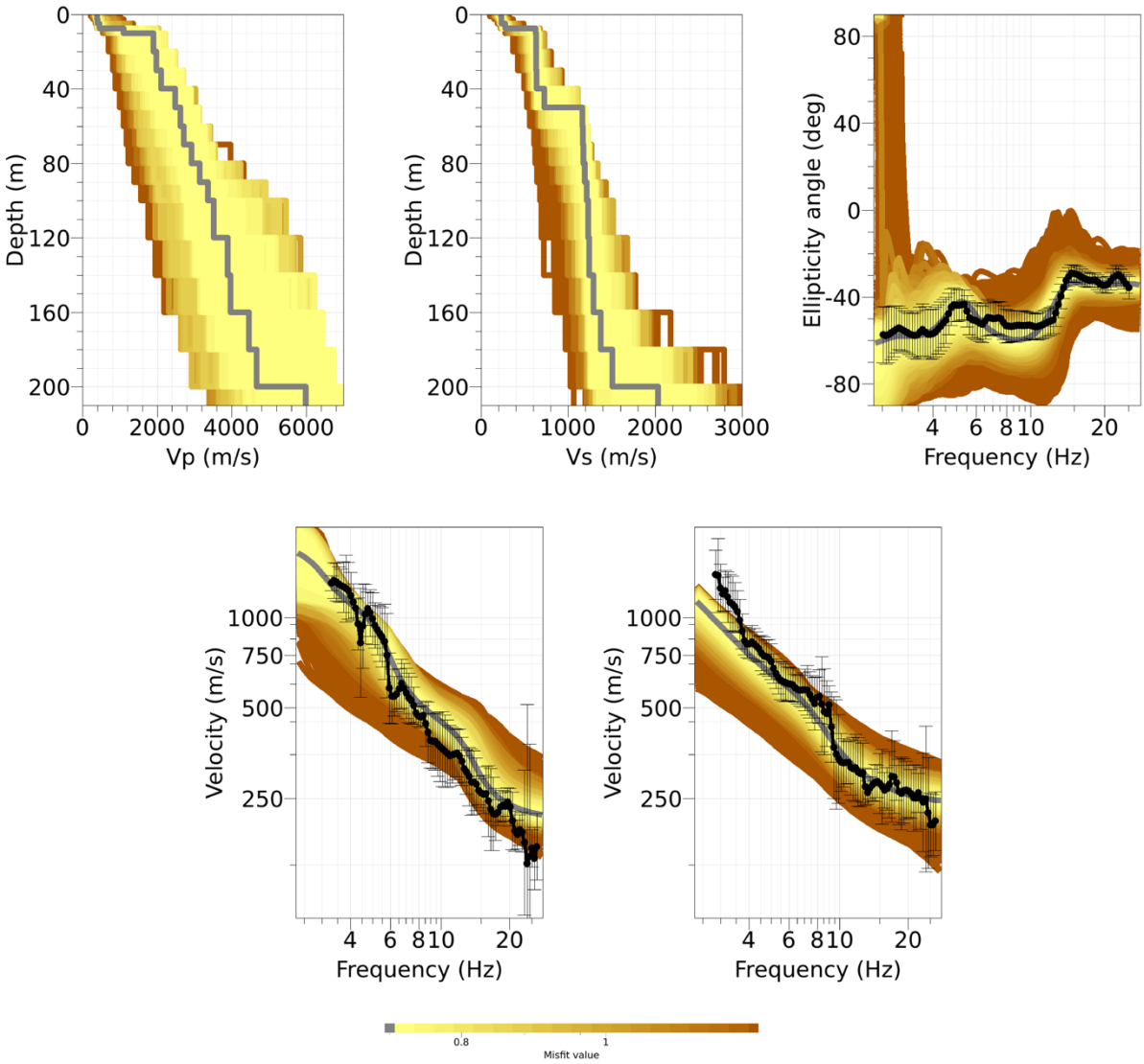

Figure 17: Inversion SZIM fix. Top line: P-wave velocity profiles (left), S-wave velocity profiles (center) and Ellipticity angle (right). Bottom line: Dispersion curves for the fundamental mode of Rayleigh (left) and Love (right) waves. The black dots indicate the data points used for the inversion, the black bars the standard deviation of the inverted curve, while the gray line shows the best-fitting model.

4.4 Inversion results - Neopsy

In addition to the five inversions performed using the Dinver routine, the inversion is performed using the multizonal transdimentional Bayesian formulation (Neopsy – Hallo et al. 2021). The targets, as reported in Table 1, are the fundamental mode of Rayleigh and Love wave dispersion curves and the fundamental mode of Rayleigh wave ellipticity curve. The parametrization defined for this inversion doesn't request the number of layers but ranges for the seismic velocities, density, Poisson's ratio and depth. The S- and P-wave velocities are allowed to range from 50 to 3000 m/s and from 100 to 7500 m/s, respectively. The density is allowed to adjust between 2000 and 3000 kg/m^3, while the Poisson's ratio is set between 0.2 and 0.45. The maximum depth is 250 m and the velocity inversion is allowed at all depths. The inversion produced 5000 initial models and 25000 new models for a total of 30000 models.

The results of the inversion are shown in Fig. 18 for the Rayleigh and Love wave dispersion curves and the Rayleigh wave ellipticity curve. In Fig. 19, the posterior marginal Probability Density Function (PDF) and the resulting profiles are shown for each parameter: v_p, v_s, ρ and ν. The blue profile shows the results for the best model using the Maximum Likelihood (ML), while in magenta is represented the model with the Maximum A Posteriori (MAP) probability.

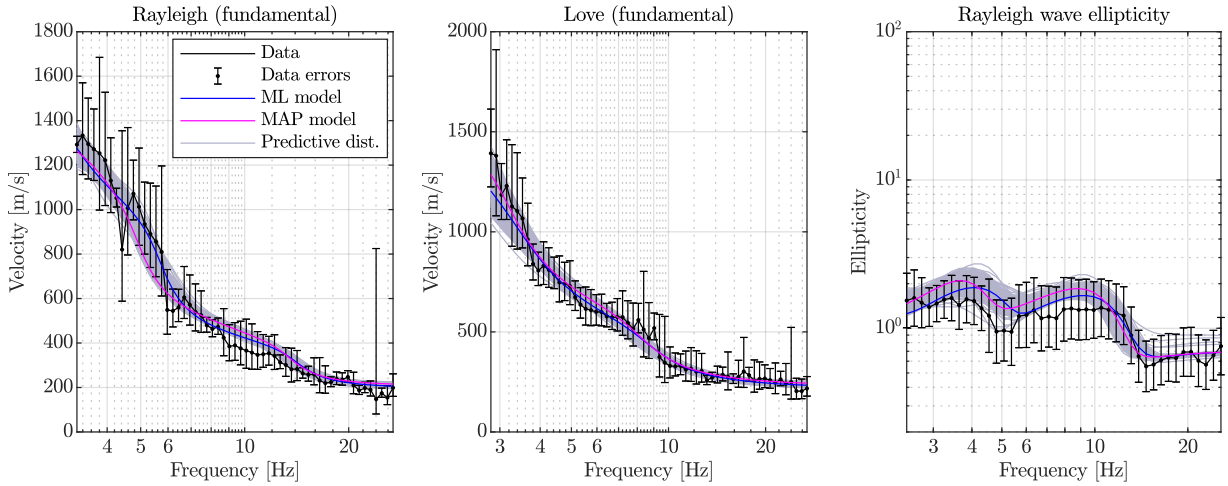

Figure 18: Results for the inversion using multizonal transdimensional Bayesian formulation. From left to right: the Rayleigh wave fundamental mode, Love wave fundamental mode and the Rayleigh wave ellipticity curve.

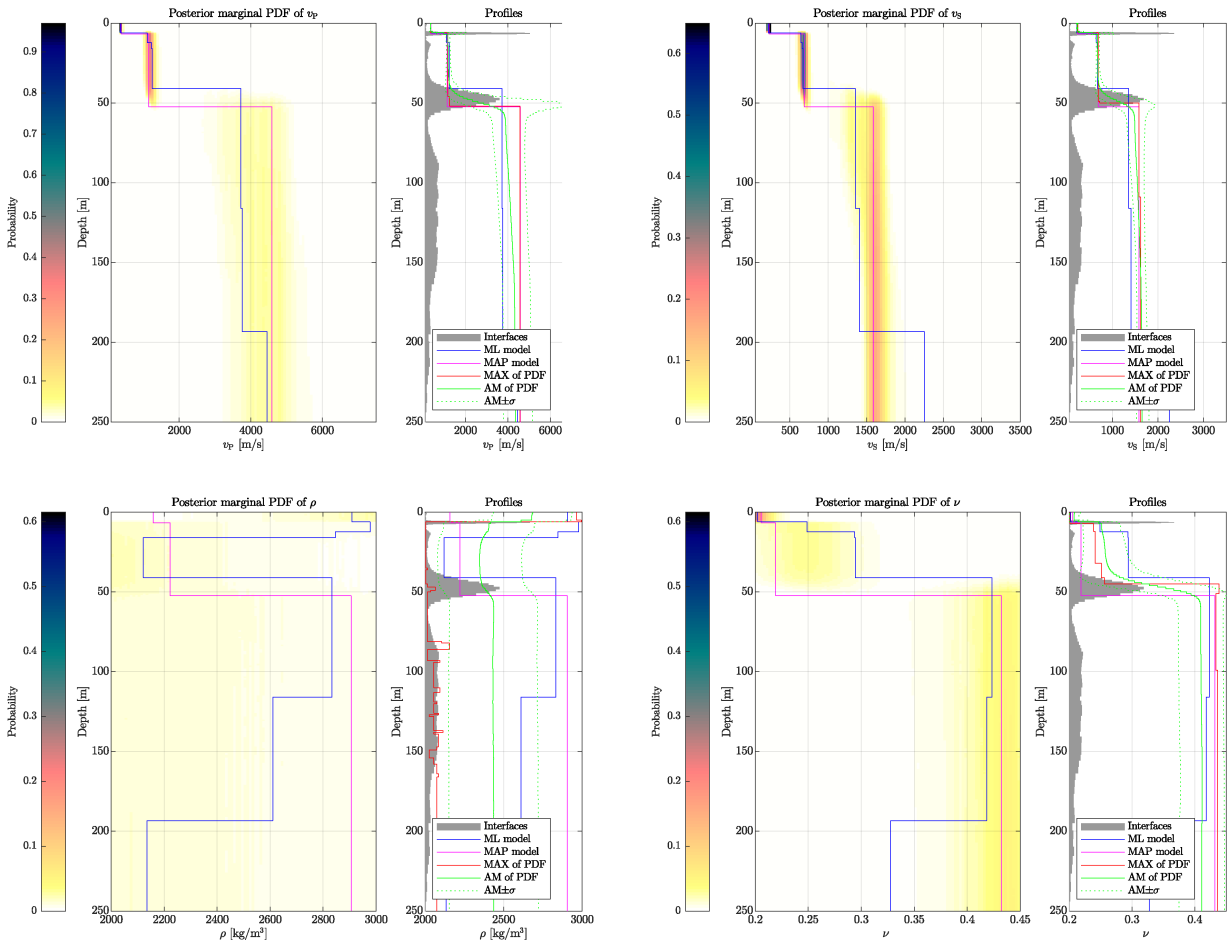

Figure 19: Posterior marginal PDF and profiles of V_p (top left), V_s (top right), density (bottom left) and Poisson's ratio (bottom right). Overview of the best profiles for each PDF for the Maximum Likelihood model (ML) and the Maximum A Posteriori model (MAP).

4.5 Discussion of the inversion results

The best-fitting models from each inversion of *dinver* and Neopsy are shown in Fig. 20.
In the first 30 meters, one shallow interface located at about 6.5 m is visible in all velocity profiles. The S-wave velocities of this interface range from 622 m/s to 688 m/s. A second interface is located at about 48 m. This, recognized by all profiles, has S-wave velocities of about 1278 m/s in *dinver*, 1355 m/s in ML model and 1587 m/s for the MAP model. A third and last interface corresponding to the transition to the half-space is identified by the *dinver* profiles and the ML model. It is located between 167.6 and 193.4 m and has S-wave velocities between 1790 m/s and 2254 m/s. While *SZIM 3l, SZIM 5l, SZIM 7l* and *ML* show a strong transition to the half-space, *SZIM 9l* has a smoother transition represented by two smaller interfaces.
The velocity profile obtained using the fix layers parametrization (*SZIM fix*) shows a constant increase of velocity with depth. This profile shows the two shallow interfaces at 6.4 and 50 meters. The third interface, the half-space, is located at 200 meters and the S-wave velocity is 2033 m/s. It is located a bit deeper than all the other velocity profiles but with similar velocities.

The velocity profiles resulting from the inversions in *dinver* have V_{S30} between 453.99 and 460.19 m/s, the MAP model has a V_{S30} of 477.59 m/s and the ML model of 470. 89 m/s. The average V_{S30} for the estimated profiles is 462.1 ± 8.81 m/s.

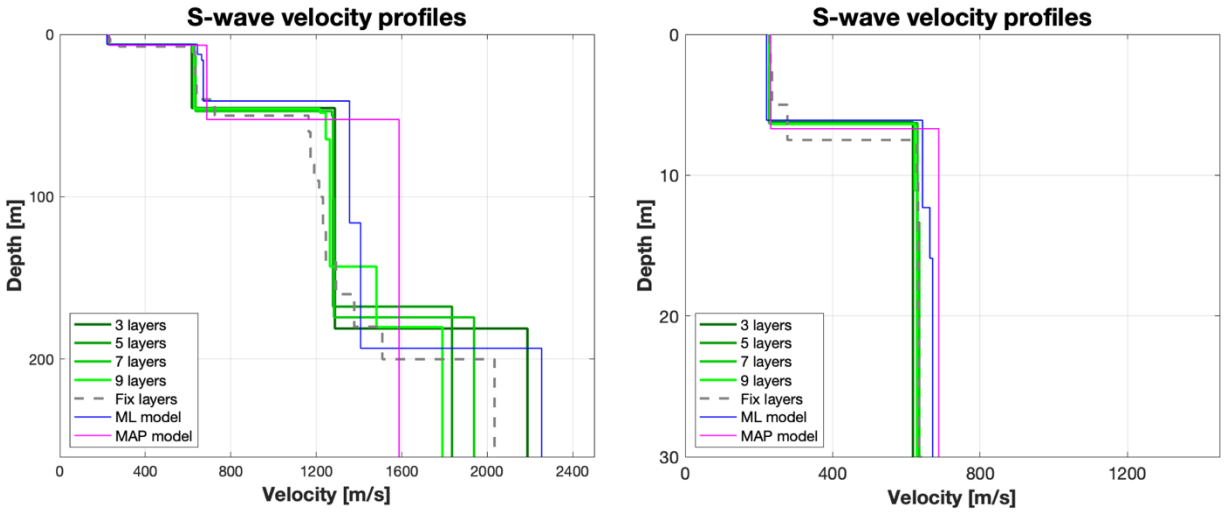

Figure 20: Overview of the best shear-wave velocity profiles of the different inversions (left) and zoom on the upper 3 0 m of the inversion profiles.

5 Further results from the inverted profiles

5.1 SH transfer function

In Figure 21, the average theoretical shear-wave transfer function for the best models of all five parametrization, for the MAP and ML models and the empirical amplification at SZIM station are shown. For the investigated site, the best *dinver* models predict an average amplification between 1.0 and 5.5 with the maximum at 8.7 Hz. The MAP and ML models in magenta and blue colors, respectively, are similar in terms of shape to the *dinver* results but they are shifted to lower and higher frequencies.

The present (27.01.2022) empirical amplification is calculated using a maximum of 50 earthquakes between 1.6 and 6.8 Hz decreasing to 17 at 0.5 Hz and to 7 at 23.4 Hz. Between 0.5 and 1.6 Hz, the empirical amplification function decreases to 0.47 increasing to 2.3 at 2.6 Hz. The amplification function has almost constant values between 1-2 in the frequency range 2.4 and 14.3 Hz, where its value start to decrease to 0.5. The theoretical shear-wave transfer functions for *dinver* (black curve), ML model and MAP model are within the standard deviation curves defined for the empirical curve (2.3 – 22.3 Hz). At lower and higher frequencies, due to the deviation of the empirical amplification function towards lower amplification values the curve referenced to the Swiss profile and the Neopsy models are out of the standard deviation curves.

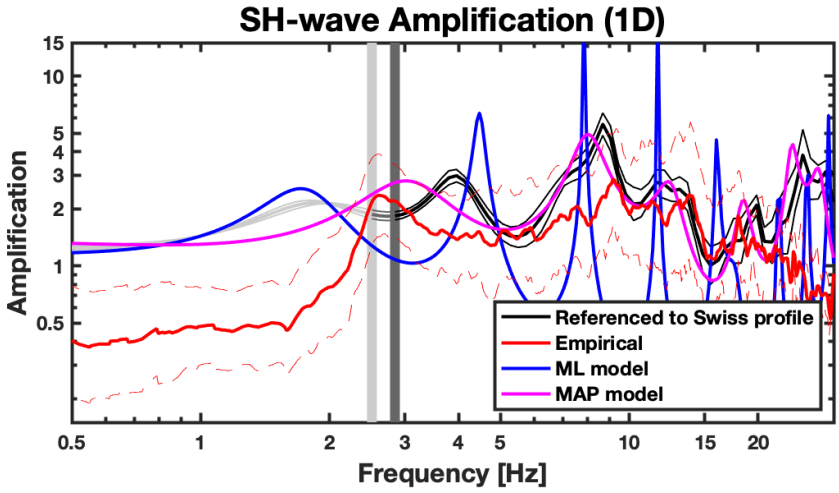

Figure 21: Modeled amplification function and standard deviation (black lines). Red curves represent the empirical amplification (solid line) and its standard deviation (dashed lines) function at the SZIM station. The empirical amplification functions for the MAP and ML models are shown by the magenta and blue curves.

5.2 Quarter-wavelength representation

The quarter-wavelength velocity approach (Joyner et al., 1981) provides, for a given frequency, the average velocity at a depth corresponding to 1/4 of the wavelength of interest. Figure 22 shows the quarter-wavelength results for the best models of inversion using the fundamental modes of Rayleigh and Love wave dispersion curves and the Rayleigh wave ellipticity angle curve (Figs. 13-17). The results using this proxy, considering frequency limits of the experimental data between 2.81 and 26.88 Hz for the dispersion curves and between 2.46 and 25.6 Hz for the ellipticity curve, is well constrained down to 60 meters using the dispersion curves and down to about 44 meters using the ellipticity curve. The quarter-wavelength impedance contrast introduced by Poggi et al. (2012) is also displayed in the figure. It corresponds to the ratio between two quarter-wavelength average velocities, respectively from the top and the bottom part of the velocity profile, at a given frequency.

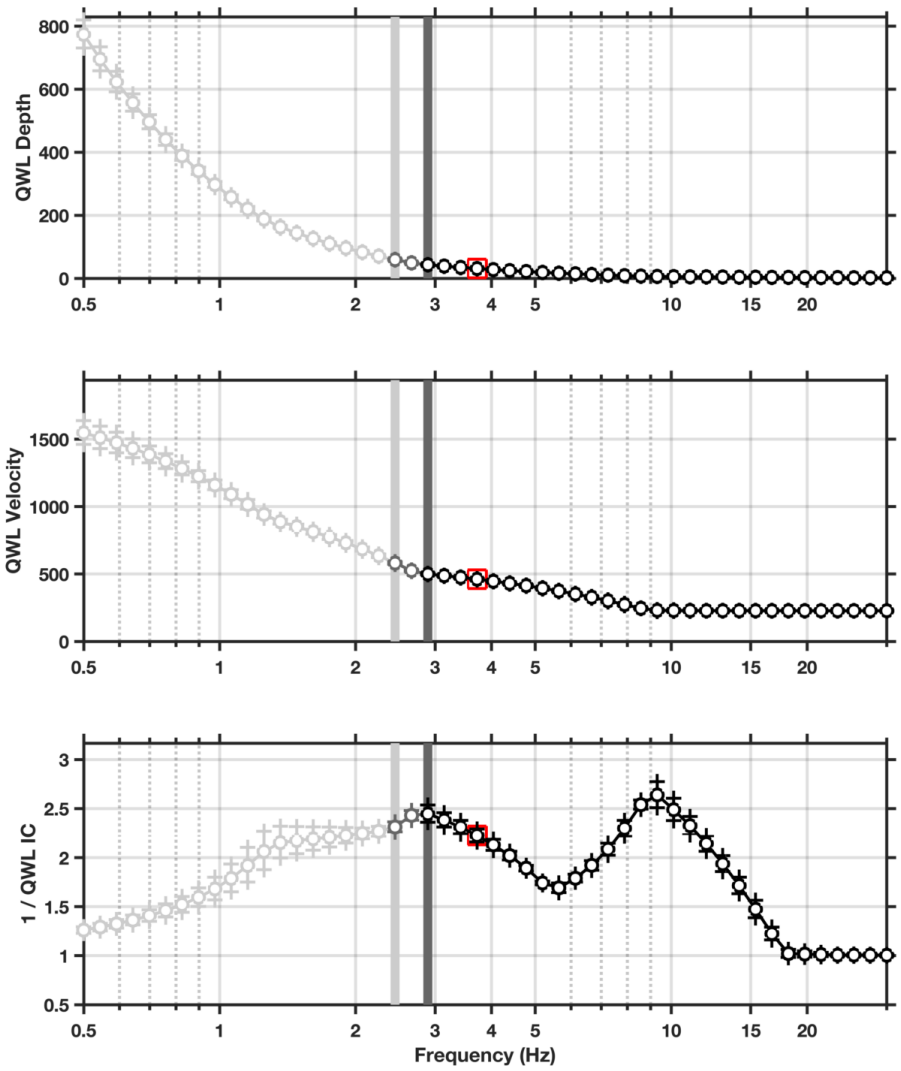

Figure 22: Quarter wavelength representation of the velocity profiles for the best models of the inversions (top: depth, center: velocity, bottom: impedance contrast). The grey light bar shows ellipticity lower frequency value, dark grey bar indicates lower frequency value obtained with dispersion curves and red square corresponds to f_{30} (frequency related to the depth of 30 m).

6 Discussion and conclusions

The passive array measurement performed in Zinal in July 2021 allowed the investigation of the subsurface underneath the SZIM station.

The H/V analysis pointed out that the is not perfectly homogeneous, probably due to the morphology of the valley. Anyway, the analysis identified two peaks in the H/V curves corresponding to two impedance contrasts: one at 3-3.9 Hz and the other between 8.6 and 15.0 Hz. A third and smaller peak is visible at low frequency at about 0.45 Hz; it was not picked since not visible in the spectra.

The inversion of Rayleigh and Love wave dispersion curves and of the Rayleigh wave ellipticity curve is performed using *dinver* and Neopsy methods. Both techniques yield to the estimation of P- and S-wave velocity profiles investigating the subsurface down to about 200 m. All *dinver* velocity profiles show three interfaces at about 6.5, 48 and 167-193 meters. This last corresponds to the transition to the half-space and has S-wave velocities between 1790 and 2254 m/s. *SZIM 9l* is the only velocity profile showing a smooth transition to the bedrock. The velocity profile obtained using the fix layers parametrization *(SZIM fix*) shows two interfaces in the first 50 meters with the transition to the half-space at 200 m. The MAP model from Neopsy identifies the two shallow interfaces but not the half-space. The V_{S30} value for the site is 460.19 m/s, corresponding to soil class B in EC8 and C in SIA261 classifications.
The theoretical shear-wave transfer function predicts an amplification function between 1.3 and 1.8 between 0.5 and 2.4 Hz. At higher frequencies, the curve shows peaks and troughs with amplification between 0.9 and 5.5. The comparison of theoretical shear-wave transfer function for the *dinver* and Neopsy models and the empirical amplification function show a quite good agreement in the frequency range 2.3 – 22.3 Hz. At lower and higher frequencies, the empirical function presents values that are much lower than the theoretic shear-wave transfer function, probably due to the low number of recorded events.

References

Burjánek, J., Gassner-Stamm, G., Poggi, V., Moore, J. R., and Fäh, D. (2010). Ambient vibration analysis of an unstable mountain slope. Geophys. J. Int., 180:820–828.

Burjánek, J., Moore, J. R., Molina, F. X. Y., and Fäh, D. (2012). Instrumental evidence of normal mode rock slope vibration. Geophys. J. Int., 188:559–569.

Fäh, D., Gardini, D., et al. (2003). Earthquake Cataloque of Switzerland (ECOS) and the related macroseismic database. Eclogae geol. Helv. 96.

Fäh, D., Wathelet, M., Kristekova, M., Havenith, H., Endrun, B., Stamm, G., Poggi, V., Burjanek, J., and Cornou, C. (2009). Using ellipticity information for site characterisation. NERIES deliverable JRA4 D4, available at http://www.neries-eu.org.

Fritsche, S., Fäh, D., Gisler, M., and Giardini, D. (2006). Reconstructing the damage field of the 1855 earthquake inSwitzerland: historical investigations on a well-documented event Geophys. J. Int. (2006)166, 719–731

Hobiger, M., Bard, P.-Y., Cornou, C., and Le Bihan, N. (2009). Single station determination of Rayleigh wave ellipticity by using the random decrement technique (RayDec). Geophys. Res. Lett., 36.

Maranò, S., Reller, C., Loeliger, H.-A., and Fäh, D. (2012). Seismic waves estimation and wavefield decomposition: Application to ambient vibrations. Geophys. J. Int., 191:175–188.

Poggi, V. and Fäh, D. (2010). Estimating Rayleigh wave particle motion from three component array analysis of ambient vibrations. Geophys. J. Int., 180:251–267.

Poggi, V., Edwards, B., and Fäh, D. (2010). Characterizing the Vertical-to-Horizontal Ratio of Ground Motion at Soft-Sediment Sites. Bulletin of the Seismological Society of America, 102(6): 2741 2756.

Wathelet, M., Chatelain, J.-L., Cornou, C., Di Giulio, G., Guillier, B., Ohrnberger, M. and Savvaidis, A. (2020). Geopsy: A User-Friendly Open-Source Tool Set for Ambient Vibration Processing. Seismological Research Letters, **91**(3), 1878--1889, doi: 10.1785/0220190360.